Review Vol. 8, No. 2 | 1 Feb 2017 | BIOMEDICAL OPTICS EXPRESS 622

Biomedical Optics EXPRESS

En face coherence microscopy [Invited]

OLIVIER THOUVENIN,[1] KATE GRIEVE,[2] PENG XIAO,[1] CLEMENT APELIAN,[1,3] AND A. CLAUDE BOCCARA[1]

[1] *Institut Langevin ESPCI, PSL Research University, CNRS UMR7587 1rue Jussieu, Paris F75005, France*
[2] *CHNO des Quinze Vingts/Institut de la Vision, 28 rue de Charenton, Paris F75012, France*
[3] *LLTech Pépinière Paris Santé Cochin 29 rue du Faubourg Saint Jacques Paris F75014, France*
[*] *claude.boccara@espci.fr*

Abstract: *En face* coherence microscopy or flying spot or full field optical coherence tomography or microscopy (FF-OCT/FF-OCM) belongs to the OCT family because the sectioning ability is mostly linked to the source coherence length. In this article we will focus our attention on the advantages and the drawbacks of the following approaches: *en face* versus B scan tomography in terms of resolution, coherent versus incoherent illumination and influence of aberrations, and scanning versus full field imaging. We then show some examples to illustrate the diverse applications of *en face* coherent microscopy and show that endogenous or exogenous contrasts can add valuable information to the standard morphological image. To conclude we discuss a few domains that appear promising for future development of *en face* coherence microscopy.

OCIS codes: (170.1650) Coherence imaging; (180.1655) Coherence tomography; (180.3170) Interference microscopy; (120.5820) Scattering measurements; (170.4580) Optical diagnostics for medicine.

References and links

1. B. P. Abbott, R. Abbott, F. Acernese, Group Author(s): LIGO Sci Collaboration; Virgo Collaboration. An upper limit of the stochastic gravitational-wave background of cosmological origin. Nature; Volume: 460 Issue: 7258 Pages: 990–994 Published: AUG 20 2009.
2. E. Beaurepaire, A. C. Boccara, M. Lebec, L. Blanchot, and H. Saint-Jalmes, "Full-field optical coherence microscopy," Opt. Lett. **23**(4), 244–246 (1998).
3. J. A. Izatt, M. R. Hee, G. M. Owen, E. A. Swanson, and J. G. Fujimoto, "Optical coherence microscopy in scattering media," Opt. Lett. **19**(8), 590–592 (1994).
4. Optical Coherence Tomography Technology and Applications Editors: W. Drexler and J.G. Fujimoto (Online).
5. A. Dubois, L. Vabre, A. C. Boccara, and E. Beaurepaire, "High-resolution full-field optical coherence tomography with a Linnik microscope," Appl. Opt. **41**, 805–812 (2002).
6. L. Vabre, A. Dubois, and A. C. Boccara, "Thermal-light full-field optical coherence tomography," Opt. Lett. **27**(7), 530–532 (2002).
7. Handbook of Full-Field Optical Coherence Microscopy: Technology and Applications; Arnaud Dubois editor. Pan Stanford 2016.
8. M. Akiba, K. P. Chan, and N. Tanno, "Full-field optical coherence tomography by two-dimensional heterodyne detection with a pair of CCD cameras," Opt. Lett. **28**(10), 816–818 (2003).
9. L. Yu and M. Kim, "Full-color three-dimensional microscopy by wide-field optical coherence tomography," Opt. Express **12**(26), 6632–6641 (2004).
10. Y. Watanabe, Y. Hayasaka, M. Sato, and N. Tanno, "Full-field optical coherence tomography by achromatic phase shifting with a rotating polarizer," Appl. Opt. **44**(8), 1387–1392 (2005).
11. W. Y. Oh, B. E. Bouma, N. Iftimia, S. H. Yun, R. Yelin, and G. J. Tearney, "Ultrahigh-resolution full-field optical coherence microscopy using InGaAs camera," Opt. Express **14**(2), 726–735 (2006).
12. M. Pircher, E. Götzinger, and C. K. Hitzenberger, "Dynamic focus in optical coherence tomography for retinal imaging," J. Biomed. Opt. **11**(5), 054013 (2006).
13. John Holmes and Julia Welzel; OCT in Dermatology chapter 73 of reference 4.
14. https://vivosight.com/about-us/product/
15. Z. Ding, H. Ren, Y. Zhao, J. S. Nelson, and Z. Chen, "High-resolution optical coherence tomography over a large depth range with an axicon lens," Opt. Lett. **27**(4), 243–245 (2002).
16. R. A Leitgeb, T. Lasser, and M. Villiger; OCM with Engineered Wavefront; chapter 29 of ref. 4.
17. T. S. Ralston, D. L. Marks, P. S. Carney, and S. A. Boppart, "Interferometric synthetic aperture microscopy," Nat. Phys. **3**(2), 129–134 (2007).
18. Adolf F. Fercher; Inverse Scattering and Aperture Synthesis in OCT; chapter 4 of reference 4.

#279912 http://dx.doi.org/10.1364/BOE.8.000622
Journal © 2017 Received 1 Nov 2016; revised 29 Dec 2016; accepted 31 Dec 2016; published 6 Jan 2017

19. A. Ahmad, N. D. Shemonski, S. G. Adie, H.-S. Kim, W.-M. W. Hwu, P. S. Carney, and S. A. Boppart, "Real-time in vivo computed optical interferometric tomography," Nat. Photonics **7**(6), 444–448 (2013).
20. Y.-Z. Liu, D. N. Shemonski, S. G. Adie, A. Ahmad, A. J. Bower, P. S. Carney and S. A. Boppart, "Computed optical interferometric tomography for high-speed volumetric cellular imaging," Biomed. Opt. Express **5**(9), 2988 (2014).
21. N. D. Shemonski, F. A. South, Y. Z. Liu, S. G. Adie, P. S. Carney, and S. A. Boppart, "Computational high-resolution optical imaging of the living human retina," Nat. Photonics **9**(7), 440–443 (2015).
22. A. Kumar, T. Kamali, R. Platzer, A. Unterhuber, W. Drexler, and R. A. Leitgeb, "Anisotropic aberration correction using region of interest based digital adaptive optics in Fourier domain OCT," Biomed. Opt. Express **6**(4), 1124–1134 (2015).
23. A. Kumar, W. Drexler, and R. A. Leitgeb, "Subaperture correlation based digital adaptive optics for full field optical coherence tomography," Opt. Express **21**(9), 10850–10866 (2013).
24. A. Kumar, W. Drexler, and R. A. Leitgeb, "Numerical focusing methods for full field OCT: a comparison based on a common signal model," Opt. Express **22**(13), 16061–16078 (2014).
25. A. Podoleanu, J. Rogers, D. Jackson, and S. Dunne, "Three dimensional OCT images from retina and skin," Opt. Express **7**(9), 292–298 (2000).
26. A. D. Aguirre, C. Zhou, H. C. Lee, O. O. Ahsen, and J. G. Fujimoto, Optical Coherence Microscopy. Chapter 28 of reference 4.
27. R. B. Rosen, P. Garcia, A. G. Podoleanu, R. Cucu, G. Dobre, I. Trifanov, M. E. J. V. Velthoven, M. D. de Smet, J. A. Rogers, M. Hathaway, J. Pedro, and R. Weitz; En-face Flying Spot OCT/Ophthalmoscope. Chapter 59 of Reference 4.
28. A. F. Fercher, C. K. Hitzenberger, M. Sticker, E. Moreno-Barriuso, R. Leitgeb, W. Drexler, and H. Sattmann, "A thermal light source technique for optical coherence tomography," Opt. Commun. **185**(1-3), 57–64 (2000).
29. W. Drexler, Y. Chen, A. D. Aguirre, B. Považay, A. Unterhuber, and J. G. Fujimoto, Ultrahigh Resolution Optical Coherence Tomography, Chapter 9 of Reference 4.
30. V. J. Srinivasan, T. H. Ko, M. Wojtkowski, M. Carvalho, A. Clermont, S. E. Bursell, Q. H. Song, J. Lem, J. S. Duker, J. S. Schuman, and J. G. Fujimoto, "Noninvasive volumetric imaging and morphometry of the rodent retina with high-speed, ultrahigh-resolution optical coherence tomography," Invest. Ophthalmol. Vis. Sci. **47**(12), 5522–5528 (2006).
31. K. Bizheva, A. Unterhuber, B. Hermann, B. Povazay, H. Sattmann, A.F. Fercher, W. Drexler, M. Preusser, H. Budka, A. Stingl, T. Le, "Imaging ex vivo healthy and pathological human brain tissue with ultra-high-resolution optical coherence tomography," J. Biomed. Opt. **10**, 11006 (2005)
32. K. Bizheva, A. Unterhuber, B. Hermann, B. Povazay, H. Sattmann, W. Drexler, A. Stingl, T. Le, M. Mei, R. Holzwarth, H. A. Reitsamer, J. E. Morgan, and A. Cowey, "Imaging ex vivo and in vitro brain morphology in animal models with ultrahigh resolution optical coherence tomography," J. Biomed. Opt. **9**(4), 719–724 (2004).
33. G. S. Kino and S. S. C. Chim, "Mirau correlation microscope," Appl. Opt. **29**(26), 3775–3783 (1990).
34. http://www.lltechimaging.com/category/news-press/news-list/
35. https://www.thorlabs.com/newgrouppage9.cfm?objectgroup_id=5702
36. K. Grieve, M. Paques, A. Dubois, J. Sahel, C. Boccara, and J.-F. Le Gargasson, "Ocular Tissue Imaging Using Ultrahigh-Resolution, Full-Field Optical Coherence Tomography," Invest. Ophthalmol. Vis. Sci. **45**(11), 4126–4131 (2004).
37. K. Grieve, A. Dubois, M. Simonutti, M. Paques, J. Sahel, J.-F. Le Gargasson, and C. Boccara, "*In vivo* anterior segment imaging in the rat eye with high speed white light full-field optical coherence tomography," Opt. Express **13**(16), 6286–6295 (2005).
38. High resolution in-vivo imaging of skin with full-field optical coherence tomography, Dalimier, E Proceedings of SPIE 8926–89260P (2014).
39. D. D. Nolte, K. Jeong, J. Turek, and P. M. W. French, Holographic Optical Coherence Imaging Chapter 30 of reference 4.
40. C. Dunsby, D. Mayorga-Cruz, I. Munro, Y. Gu, P. M. W. French, D. D. Nolte, and M. R. Melloch, "High-speed wide-field coherence-gated imaging via photorefractive holography withphotorefractive multiple quantum well devices," J. Opt. A, Pure Appl. Opt. **5**(6), S448–S456 (2003).
41. P. Massatsch, F. Charrière, E. Cuche, P. Marquet, and C. D. Depeursinge, "Time-domain optical coherence tomography with digital holographic microscopy," Appl. Opt. **44**(10), 1806–1812 (2005).
42. D. Hillmann, G. Franke, L. Hinkel, B. P. K. Tim, and G. Hüttmann, "Off-axis full-field swept-source optical coherence tomography using holographic refocusing," Proc. SPIE **8571**, 857104 (2013).
43. H. Sudkamp, P. Koch, H. Spahr, D. Hillmann, G. Franke, M. Münst, F. Reinholz, R. Birngruber, and G. Hüttmann, "*In-vivo* retinal imaging with off-axis full-field time-domain optical coherence tomography," Opt. Lett. **41**(21), 4987–4990 (2016).
44. M. Villiger, C. Pache, and T. Lasser, "Dark-field optical coherence microscopy," Opt. Lett. **35**(20), 3489–3491 (2010).
45. E. Auksorius and A. C. Boccara, "Dark-field full-field optical coherence tomography," Opt. Lett. **40**(14), 3272–3275 (2015).
46. B. Hermann, E. J. Fernández, A. Unterhuber, H. Sattmann, A. F. Fercher, W. Drexler, P. M. Prieto, and P. Artal, "Adaptive-optics ultrahigh-resolution optical coherence tomography," Opt. Lett. **29**(18), 2142–2144 (2004).
47. Robert J. Zawadzki and D. T. Miller. Retinal AO OCT in Chapter 61 of Reference 4.

48. Y. Zhang, B. Cense, J. Rha, R. S. Jonnal, W. Gao, R. J. Zawadzki, J. S. Werner, S. Jones, S. Olivier, and D. T. Miller, "High-speed volumetric imaging of cone photoreceptors with adaptive optics spectral-domain optical coherence tomography," Opt. Express **14**(10), 4380–4394 (2006).
49. D. Merino, C. Dainty, A. Bradu, and A. G. Podoleanu, "Adaptive optics enhanced simultaneous en-face optical coherence tomography and scanning laser ophthalmoscopy," Opt. Express **14**(8), 3345–3353 (2006).
50. M. Rueckel, J. A. Mack-Bucher, and W. Denk, "Adaptive wavefront correction in two-photon microscopy using coherence-gated wavefront sensing," Proc. Natl. Acad. Sci. U.S.A. **103**(46), 17137–17142 (2006).
51. B. Karamata, P. Lambelet, M. Laubscher, R. P. Salathé, and T. Lasser, "Spatially incoherent illumination as a mechanism for cross-talk suppression in wide-field optical coherence tomography," Opt. Lett. **29**(7), 736–738 (2004).
52. B. Karamata, M. Laubscher, M. Leutenegger, S. Bourquin, T. Lasser, and P. Lambelet, "Multiple scattering in optical coherence tomography. I. Investigation and modeling," J. Opt. Soc. Am. A **22**(7), 1369–1379 (2005).
53. B. Karamata, M. Leutenegger, M. Laubscher, S. Bourquin, M. Laubscher, S. Bourquin, T. Lasser, and P. Lambelet, "Multiple scattering in optical coherence tomography. II. Experimental and theoretical investigation of cross talk in wide-field optical coherence tomography," J. Opt. Soc. Am. A **22**(7), 1380–1388 (2005).
54. P. Xiao, M. Fink, and A. C. Boccara, "Full-field spatially incoherent illumination interferometry: a spatial resolution almost insensitive to aberrations," Opt. Lett. **41**(17), 3920–3923 (2016).
55. P. Xiao, M. Fink, and A. C. Boccara, "Adaptive optics full-field optical coherence tomography," J. Biomed. Opt. **21**(12), 121505 (2016).
56. Zhongping Chen and Shuo Tang Second Harmonic OCT and Combined MPM/OCT chapter 49 of reference 4.
57. A. S. Nam, B. Vakoc, D. Blauvelt, and I. C. Calero ; Optical Coherence Tomography in Cancer Imaging Chapter 45 of reference 4.
58. Chao Zhou, David W. Cohen, Y. Wang, H. C. Lee, A. E. Mondelblatt, T. H. Tsai, A. D. Aguirre, J. G. Fujimoto and J. L. Connolly, Integrated Optical Coherence Tomography and Microscopy for *Ex Vivo* Multiscale Evaluation of Human Breast Tissues. Cancer Res; 70 (24) December 15, 2010.
59. Eugenie Dalimier, Osnath Assayag, Fabrice Harms, and A. Claude Boccara; Assessment of Breast, Brain and Skin Pathological Tissue Using Full Field OCM Chapter 26 of reference 4.
60. http://www.lltechimaging.com/image-gallery/clinical-applications/
61. O. Assayag, M. Antoine, B. Sigal-Zafrani, M. Riben, F. Harms, A. Burcheri, K. Grieve, E. Dalimier, B. Le Conte de Poly, and C. Boccara, "Large field, high resolution full field optical coherence tomography: a pre-clinical study of human breast tissue and cancer assessment. Technology in cancer research and treatment," TCRT: Express **1**(1), 21–34 (2013).
62. I. T. A. Peters, P. L. Stegehuis, R. Peek, F. L. Boer, E. W. V. Zwet, J. Eggermont, J. R. Westphal, P. J. K. Kuppen, J. B. M. Z. Trimbos, C. G. J. M. Hilders, B. P. F. Lelieveldt, C. J. H. V. de Velde, T. Bosse, J. Dijkstra, A. L. Vahrmeijer, Clinical Cancer Research: *Non-invasive detection of metastases and follicle density in ovarian tissue using full-field optical coherence tomography* clincanres-0288, May 2016.
63. M. V. Sarunic, S. Weinberg, and J. A. Izatt, "Full-field swept-source phase microscopy," Opt. Lett. **31**(10), 1462–1464 (2006).
64. K. Grieve, K. Mouslim, O. Assayag, E. Dalimier, F. Harms, A. Bruhat, C. Boccara, and M. Antoine, "Assessment of Sentinel Node Biopsies With Full-Field Optical Coherence Tomography," Technol. Cancer Res. Treat. **15**(2), 266–274 (2016).
65. K. Wiesauer, M. Pircher, E. Götzinger, S. Bauer, R. Engelke, G. Ahrens, G. Grützner, C. Hitzenberger, and D. Stifter, "En-face scanning optical coherence tomography with ultra-high resolution for material investigation," Opt. Express **13**(3), 1015–1024 (2005).
66. D. Stifter Nondestructive Material Testing Using OCT. Chapter 83 of Reference 4.
67. L. Vabre, V. Loriette, A. Dubois, and J. Moreau, A.C. Boccara, "Imagery of local defects in multilayer components by short coherence length interferometry," Opt. Lett. **27**(21), 1899–1901 (2002).
68. L. N. Darlow, J. Connan, and S. S. Akhoury, "Internal fingerprint zone detection in optical coherence tomography fingertip scans," ELECTIM **24**, 023027 (2015).
69. L. N. Darlow and J. Connan, "Study on internal to surface fingerprint correlation using optical coherence tomography and internal fingerprint extraction," ELECTIM **24**, 063014 (2015).
70. W. Wieser, B. R. Biedermann, T. Klein, C. M. Eigenwillig, and R. Huber, "Multi-megahertz OCT: High quality 3D imaging at 20 million A-scans and 4.5 GVoxels per second," Opt. Express **18**(14), 14685–14704 (2010).
71. M.-R. Nasiri-Avanaki, A. Meadway, A. Bradu, R. M. Khoshki, A. Hojjatoleslami, and A. G. Podoleanu, "Anti-spoof reliable biometry of fingerprints using en-face optical coherence tomography," Opt. Photonics J. **1**(03), 91–96 (2011).
72. E. Auksorius and A. C. Boccara, "Fingerprint imaging from the inside of a finger with full-field optical coherence tomography," Biomed. Opt. Express **6**(11), 4465–4471 (2015).
73. P. Targowski, M. Iwanicka, B. J. Rouba, and C. Frosini, OCT for Examination of Artwork chapter 82 of ref. 4.
74. http://www.oct4art.eu/
75. Science for conservation of cultural heritage French-Japanese workshop Michel Menu, Nobuyuki Kamba editor. Herman 2012.
76. E. Beaurepaire, L. Moreaux, F. Amblard, and J. Mertz, "Combined scanning optical coherence and two-photon-excited fluorescence microscopy," Opt. Lett. **24**(14), 969–971 (1999).

77. M. T. Myaing, D. J. MacDonald, and X. Li, “Fiber-optic scanning two-photon fluorescence endoscope,” Opt. Lett. **31**(8), 1076–1078 (2006).
78. J. Mavadia, J. Xi, Y. Chen, and X. Li, “An all-fiber-optic endoscopy platform for simultaneous OCT and fluorescence imaging,” Biomed. Opt. Express **3**(11), 2851–2859 (2012).
79. H. Makhlouf, A. R. Rouse, and A. F. Gmitro, “Dual modality fluorescence confocal and spectral-domain optical coherence tomography microendoscope,” Biomed. Opt. Express **2**(3), 634–644 (2011).
80. J. Mavadia-Shukla, J. F. Xi, and X. D. Li, Multi-modal endoscopy: OCT and fluorescence. *Optical Coherence Tomography: Technology and Applications,* 1599–1613. Springer International Publishing. (2015).
81. J. K. Barton, A. R. Tumlinson, and U. Utzinger, Chapter 53 of Referenec 4.
82. Integrated Optical Coherence Tomography (OCT) with Fluorescence Laminar Optical Tomography (FLOT) Chao-Wei Chen and Yu Chen Chapter 51 of Referenec 4.
83. Y. T. Pan, T. Q. Xie, C. W. Du, S. Bastacky, S. Meyers, and M. L. Zeidel, “Enhancing early bladder cancer detection with fluorescence-guided endoscopic optical coherence tomography,” Opt. Lett. **28**(24), 2485–2487 (2003).
84. A. R. Tumlinson, L. P. Hariri, U. Utzinger, and J. K. Barton, “Miniature endoscope for simultaneous optical coherence tomography and laser-induced fluorescence measurement,” Appl. Opt. **43**(1), 113–121 (2004).
85. L. P. Hariri, A. R. Tumlinson, N. H. Wade, D. G. Besselsen, U. Utzinger, E. W. Gerner, and J. K. Barton, “Ex vivo optical coherence tomography and laser-induced fluorescence spectroscopy imaging of murine gastrointestinal tract,” Comp. Med. **57**(2), 175–185 (2007).
86. S. Yuan and Y. Chen, Combining Optical Coherence Tomography with Fluorescence Imaging, Advances in Lasers and Electro Optics, Nelson Costa and Adolfo Cartaxo (Ed.), InTech (2010).
87. S. Yuan, C. A. Roney, J. Wierwille, C. W. Chen, B. Xu, G. Griffiths, J. Jiang, H. Ma, A. Cable, R. M. Summers, and Y. Chen, “Co-registered optical coherence tomography and fluorescence molecular imaging for simultaneous morphological and molecular imaging,” Phys. Med. Biol. **55**(1), 191–206 (2010).
88. S. Yuan, Q. Li, J. Jiang, A. Cable, and Y. Chen, “Three-dimensional coregistered optical coherence tomography and line-scanning fluorescence laminar optical tomography,” Opt. Lett. **34**(11), 1615–1617 (2009).
89. E. Auksorius, Y. Bromberg, R. Motiejūnaitė, A. Pieretti, L. Liu, E. Coron, J. Aranda, A. M. Goldstein, B. E. Bouma, A. Kazlauskas, and G. J. Tearney, “Dual-Modality Fluorescence and Full-Field Optical Coherence Microscopy for Biomedical Imaging Applications,” Biomed. Opt. Express **3**(3), 661–666 (2012).
90. F. Harms, E. Dalimier, P. Vermeulen, A. Fragola, and A. C. Boccara, ``Multimodal Full-Field Optical Coherence Tomography on biological tissue: toward all optical digital pathology,” Proc. SPIE BiOS, 821609 (2012).
91. H. Makhlouf, K. Perronet, G. Dupuis, S. Lévêque-Fort, and A. Dubois, “Simultaneous Optically Sectioned Fluorescence and Optical Coherence Microscopy with Full-Field Illumination,” Opt. Lett. **37**(10), 1613–1615 (2012).
92. O.Thouvenin, M.Fink, C.Boccara, ``Dynamic multimodal full-field optical coherence tomography and fluorescence microscopy,” Under revision.
93. K. Grieve, D. Ghoubay, C. Georgeon, O. Thouvenin, N. Bouheraoua, M. Paques, and V. M. Borderie, “Three-dimensional structure of the mammalian *limbal* stem cell niche,” Exp. Eye Res. **140**, 75–84 (2015).
94. K. Grieve, O. Thouvenin, A. Sengupta, V. M. Borderie, and M. Paques, “Appearance of the Retina With Full-Field Optical Coherence Tomography,” Invest. Ophthalmol. Vis. Sci. **57**(9), OCT96 (2016).
95. A. J. Rózsa, and R. W. Beuerman. “Density and Organization of Free Nerve Endings in the Corneal Epithelium of the Rabbit,” Pain **14**, 105–120 (1982).
96. C.-J. Jeon, E. Strettoi, and R. H. Masland, “The major cell populations of the mouse retina,” J. Neurosci. **18**(21), 8936–8946 (1998).
97. J. A. Izatt, M. D. Kulkarni, S. Yazdanfar, J. K. Barton, and A. J. Welch, “In vivo bidirectional color Doppler flow imaging of picoliter blood volumes using optical coherence tomography,” Opt. Lett. **22**(18), 1439–1441 (1997).
98. “J. Binding, J. B. Arous, J. F. Léger, S. Gigan, C. Boccara, and L. Bourdieu, “Brain refractive index measured *in vivo*with high-NA defocus-corrected full-field OCT and consequences for two-photon microscopy,” Opt. Express **19**, 4833–4847 (2011).
99. C. Apelian, F. Harms, O. Thouvenin, and A. C. Boccara, “Dynamic full field optical coherence tomography: subcellular metabolic contrast revealed in tissues by interferometric signals temporal analysis,” Biomed. Opt. Express **7**(4), 1511–1524 (2016).
100. F. Costello, W. Hodge, Y. I. Pan, E. Eggenberger, S. Coupland, and R. H. Kardon, “Tracking retinal nerve fiber layer loss after optic neuritis: a prospective study using optical coherence tomography,” Mult. Scler. **14**(7), 893–905 (2008).
101. K. Jeong, J. J. Turek, M. R. Melloch, and D. D. Nolte, “Functional imaging in photorefractive tissue speckle holography,” Opt. Commun. **281**(7), 1860–1869 (2008).
102. D. D. Nolte, R. An, and J. Turek, Motility Contrast Imaging and TissueDynamics Spectroscopy chapter 37 of reference 4.
103. D. D. Nolte, R. An, J. Turek, and K. Jeong, “Tissue dynamics spectroscopy for phenotypic profiling of drug effects in three-dimensional culture,” Biomed. Opt. Express **3**(11), 2825–2841 (2012).
104. D. D. Nolte, R. An, J. Turek, and K. Jeong, “Tissue dynamics spectroscopy for three-dimensional tissue-based drug screening,” J. Lab. Autom. **16**(6), 431–442 (2011).

105. M. A. Choma, A. Ellerbee, and J. A. Izatt, Ultrasensitive Phase-Resolved Imaging of Cellular Morphology and Dynamics Chapter 40 of reference 4.
106. K. J. Chalut, S. Chen, J. D. Finan, M. G. Giacomelli, F. Guilak, K. W. Leong, and A. Wax, "Label-free, high-throughput measurements of dynamic changes in cell nuclei using angle-resolved low coherence interferometry," Biophys. J. **94**(12), 4948–4956 (2008).
107. C.-E. Leroux, F. Bertillot, O. Thouvenin, and A.-C. Boccara, "Intracellular dynamics measurements with full field optical coherence tomography suggest hindering effect of actomyosin contractility on organelle transport," Biomed. Opt. Express **7**(11), 4501–4513 (2016).
108. J. Schmitt, "OCT elastography: imaging microscopic deformation and strain of tissue," Opt. Express **3**(6), 199–211 (1998).
109. R. Chan, A. Chau, W. Karl, S. Nadkarni, A. Khalil, N. Iftimia, M. Shishkov, G. Tearney, M. Kaazempur-Mofrad, and B. Bouma, "OCT-based arterial elastography: robust estimation exploiting tissue biomechanics," Opt. Express **12**(19), 4558–4572 (2004).
110. A. S. Khalil, R. C. Chan, A. H. Chau, B. E. Bouma, and M. R. K. Mofrad, "Tissue elasticity estimation with optical coherence elastography: toward mechanical characterization of in vivo soft tissue," Ann. Biomed. Eng. **33**(11), 1631–1639 (2005).
111. R. K. Wang, S. Kirkpatrick, and M. Hinds, "Phase-sensitive optical coherence elastography for mapping tissue microstrains in real time," Appl. Phys. Lett. **90**(16), 164105 (2007).
112. R. K. Wang, Z. Ma, and S. J. Kirkpatrick, "Tissue Doppler optical coherence elastography for real time strain rate and strain mapping of soft tissue," Appl. Phys. Lett. **89**(14), 144103 (2006).
113. B. F. Kennedy, T. R. Hillman, R. A. McLaughlin, B. C. Quirk, and D. D. Sampson, "In vivo dynamic optical coherence elastography using a ring actuator," Opt. Express **17**(24), 21762–21772 (2009).
114. B. F. Kennedy, X. Liang, S. G. Adie, D. K. Gerstmann, B. C. Quirk, S. A. Boppart, and D. D. Sampson, "In vivo three-dimensional optical coherence elastography," Opt. Express **19**(7), 6623–6634 (2011).
115. B. F. Kennedy, K. M. Kennedy, A. L. Oldenburg, S. G. Adie, S. A. Boppart, and D. D. Sampson, Optical Coherence Elastography Chapter 32 of reference 4.
116. A. Nahas, M. Bauer, S. Roux, and A. C. Boccara, "3D static elastography at the micrometer scale using Full Field OCT," Biomed. Opt. Express **4**, 2138–2149 (2013).
117. X. Liang, M. Orescanin, K. S. Toohey, M. F. Insana, and S. A. Boppart, "Acoustomotive optical coherence elastography for measuring material mechanical properties," Opt. Lett. **34**(19), 2894–2896 (2009).
118. X. Liang, V. Crecea, and S. A. Boppart, "Dynamic Optical Coherence Elastography: a Review," J. Innov. Opt. Health Sci. **3**(4), 221–233 (2010).
119. C. Li, G. Guan, R. Reif, Z. Huang, and R. K. Wang, "Determining elastic properties of skin by measuring surface waves from an impulse mechanical stimulus using phase-sensitive optical coherence tomography," J. R. Soc. Interface **9**(70), 831–841 (2012).
120. C. Li, G. Guan, Z. Huang, M. Johnstone, and R. K. Wang, "Noncontact all-optical measurement of corneal elasticity," Opt. Lett. **37**(10), 1625–1627 (2012).
121. S. Wang, J. Li, R. K. Manapuram, F. M. Menodiado, D. R. Ingram, M. D. Twa, A. J. Lazar, D. C. Lev, R. E. Pollock, and K. V. Larin, "Noncontact measurement of elasticity for the detection of soft-tissue tumors using phase-sensitive optical coherence tomography combined with a focused air-puff system," Opt. Lett. **37**(24), 5184–5186 (2012).
122. A. Nahas, M. Tanter, T.-M. Nguyen, J.-M. Chassot, M. Fink, and A. Claude Boccara, "From supersonic shear wave imaging to full-field optical coherence shear wave elastography," J. Biomed. Opt. **18**(12), 121514 (2013).
123. Y. Zhao, Y. Yang, R. K. Wang, and S. A. Boppart, Optical Coherence Tomographyin Tissue Engineering Chapter 64 of referenence 4.
124. A. Nahas, M. Varna, E. Fort, and A. C. Boccara, "Detection of plasmonic nanoparticles with full field-OCT: optical and photothermal detection," Biomed. Opt. Express **5**(10), 3541–3546 (2014).
125. J. A. Izatt, M. A. Choma, and A. H. Dhalla, Theory of Optical Coherence Tomography Chapter 2 of Reference 4.
126. P. E. Andersen, T. M. Jørgensen, L. Thrane, A. Tycho, and H. T. Yura, Modeling Light–Tissue Interaction in Optical Coherence Tomography Systems Chapter 3 of Refence 4.
127. J.-L. Robert and M. Fink, "Green's function estimation in speckle using the decomposition of the time reversal operator: application to aberration correction in medical imaging," J. Acoust. Soc. Am. **123**(2), 866–877 (2008).
128. A. Aubry and A. Derode, "Detection and imaging in a random medium: A matrix method to overcome multiple scattering and aberration," J. Appl. Phys. **106**(4), 044903 (2009).
129. A. Aubry and A. Derode, "Singular value distribution of the propagation matrix in random scattering media," Wave Random Complex **20**(3), 333–363 (2010).
130. A. Badon, D. Li, G. Lerosey, A. C. Boccara, M. Fink, and A. Aubry, "Smart optical coherence tomography for ultra-deep imaging through highly scattering media," Sci. Adv. **2**(11), e1600370 (2016).

1. Introduction

We would like first to apologize to those who contributed to the progress of this field that we have omitted to mention. As a group of experimental physicists tied to the challenges of optical measurements reaching their physical limits, we switched with enthusiasm from measuring the roughness of the mirrors for gravitational antennas (VIRGO-LIGO project [1]) to our first tomographic microscopy measurements [2]. The idea of jumping by 9 orders of magnitude from the least scattering media (ultrapure silica optics with a mean free path about 100 Km) to biological samples (mean free path about 100 µm) was indeed a very stimulating jump. We have to confess that this jump required very minor changes as illustrated in Fig. 1 that shows our setups: the Wollaston prism that was used for measuring roughness with a "picometer" sensitivity common path interferometer was simply replaced by a straightforward Michelson polarization interferometer. Thankfully both were shot noise limited, but the limitations of the technique were quickly revealed when using a camera instead of a single detector, as we will discuss below. Our tomographic microscopy approach was inspired by an illuminating paper about OCM, explaining and demonstrating the gain that could be expected from such an approach [3] compared to confocal microscopy, as well by the first papers on OCT [4].

Our motivation to write this paper is not to go back through historical memories in a detailed review but rather to discuss important points that, we think, have contributed to the development of en face tomo-microscopy. Hundreds of valuable references dealing with en face tomographic microscopy can be found in a number of chapters of the books edited by W. Drexler and J. Fujimoto [4]; we will refer to a few of these chapters throughout this article.

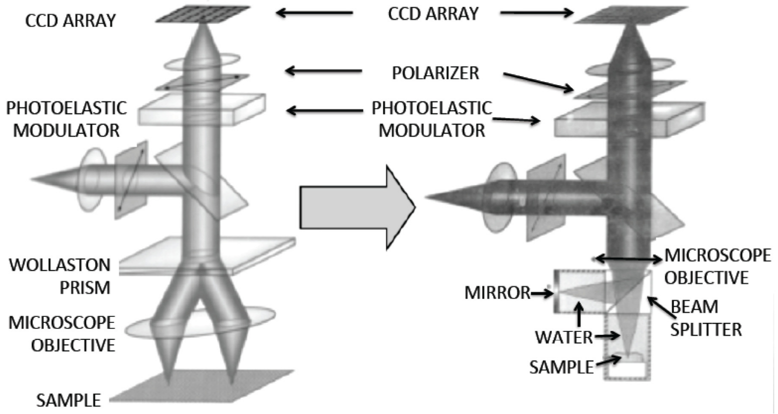

Fig. 1. From Differential Interference Contrast (DIC) to FF-OCM. Two similar versions of a polarization interferometer [2] using a photo elastic modulator and a synchronous lock-in detection.

2. *En face* versus B mode OCT/OCM: review of the principle and resolution issues

When we heard first about OCT it was said that this technique was equivalent to ultrasonography (medical ultrasound) with a wavelength 1000 times shorter, so micrometer resolution ranges rather than millimeter ones were expected. Medical ultrasound displays so-called B-scan images and so did the time domain, and later the Fourier domain (spectral as well as swept source) OCT [4]. This kind of cross-sectional depth exploration of the samples and in particular of the retina was found to be of importance to reveal pathologies and to follow up their evolution. Nevertheless doctors often asked for *en face* images that resembled their habitual fundus SLO (scanning laser ophthalmoscope) views, and, due to the progress in speed of the OCT systems such images were obtained from 3-D stacks of images within a reasonable amount of time, compatible with an eye examination. The main motivation to perform *en face* OCT is mostly to be able to get a standard microscopy resolution: for this reason we started to call it Full Field Optical Coherence Microscopy (FF-OCM) and to be sure to be adopted by the OCT community we often switched to Full Field OCT (FF-OCT) [5,6]. In this paper we will try to stick to the term OCM (full field or scanning) because the "microscopic" aspect was the main focus: while OCT features high axial resolution, OCM focuses on achieving both high lateral and axial resolution. The reader should be aware that a number of papers dealing with OCM use either the OCT or the OCM nomenclature [8,9][10,11]. For more specific information about this technique, we refer the reader to book that is entirely dedicated to various aspects of FF-OCT [7].

From the following comparison of the principle of OCT with the principle of OCM, one can easily understand the basic differences in terms of resolution (Fig. 2 and Fig. 3).

In OCT, an axial line (A-scan) is recorded first, followed by transverse scanning in order to construct a B-scan. The required depth of field imposes working with low NA objectives that correspond to the exploration depth (e.g. to cover the entire retinal thickness), thus limiting the lateral resolution. Typical OCT lateral resolutions imposed by the depth of field lie in the 10-20 µm range. For OCM approaches there is no need to work with a large depth of field because the images are acquired at a given depth. In OCM, the axial resolution is mostly imposed by the source spectrum (1 µm with thermal sources, 5-15µm with LEDs), while typical transverse resolution with high NA objectives is around 1 µm. Nevertheless we should mention that various other approaches have successfully overcome the OCT lateral resolution limitation.

Typical OCT transverse resolutions imposed by the depth of field lie in the 10-20 µm range. Nevertheless we should mention that various approaches have successfully overcome this limitation on lateral resolution:

- Dynamic focusing, that improves the resolution but decreases the speed of the recording [12]
- Multifocal multi-beam OCT introduced by Michelson Diagnostics [13,14] where the required depth of field is divided into a number of small axial zones resulting in improved resolution
- Use of Bessel beams that increase the depth of field while keeping the transverse resolution [15,16]
- Synthetic aperture OCT [17,18] that leads to a resolution in all planes that is equivalent to the resolution achieved only at the focal plane for conventional high-resolution microscopy, thus eliminating the compromise between resolution and depth of field.
- More generally, post-processing of experimental data opened up a completely new field able to revisit the standard optical views that are mostly based on geometrical optics. Here the use of coherent detection led not only to improvements in the use of synthetic aperture [18] for the extension of the depth of field by orders of magnitude, but by adding computational adaptive optics [19,20], aberration effects can also be overcome.
- *En face* images over a wide field of view that induce anisotropic aberrations, recorded with a tightly focused (<1 µm) scanning illumination spectral domain OCM, have be corrected using digital adaptive optics targeting regions of interest [21]
- Finally, numerical methods have successfully solved the problem of defocus in swept source FF-OCM coherent illumination [22]. In reference [23] not only are various algorithms compared in terms of speed and efficiency but didactic descriptions of the processes involved are provided (Fig. 4 of reference [24])

After using the first setup described in Fig. 1, we decided to use a different interferometer (Fig. 3, left) using 2 identical objectives that allow a much larger numerical aperture [5] (at that time we were not aware that it was proposed by Linnik!) and simplified the reference arm modulation by using a piezoelectric transducer.

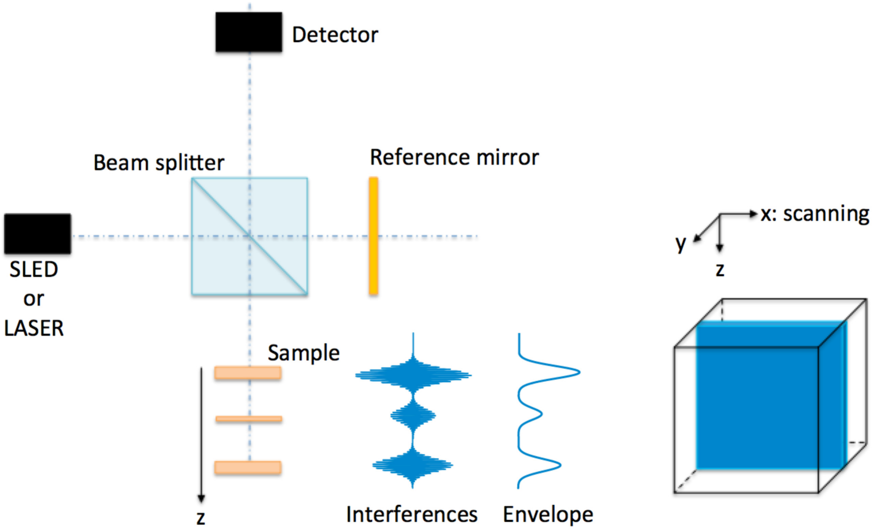

Fig. 2. OCT principle: A spatially coherent source is focused on the sample with a depth of field corresponding to the depth of the recorded volume.

The use of high NA microscope objectives imposes recording of *en face* images either by using a camera or a scanning spot (i.e. flying spot approach [25–27]), or by scanning the sample [3] in a plane perpendicular to the optical axis.

As mentioned before in terms of sectioning ability we expect a sub-micron axial resolution when using a broadband thermal source [28] with a smooth spectral distribution only achievable with sophisticated mode locked laser in the sub-five-femtosecond range [29,30] [31,32]. Single LEDs and SLDs sources offer similar axial resolution in the 10 µm range. In the case of very large NA objectives the depth of field happens to be smaller than the coherent sectioning; in this case the axial OCM sectioning is the same as that of a confocal microscope of the same numerical aperture [33].

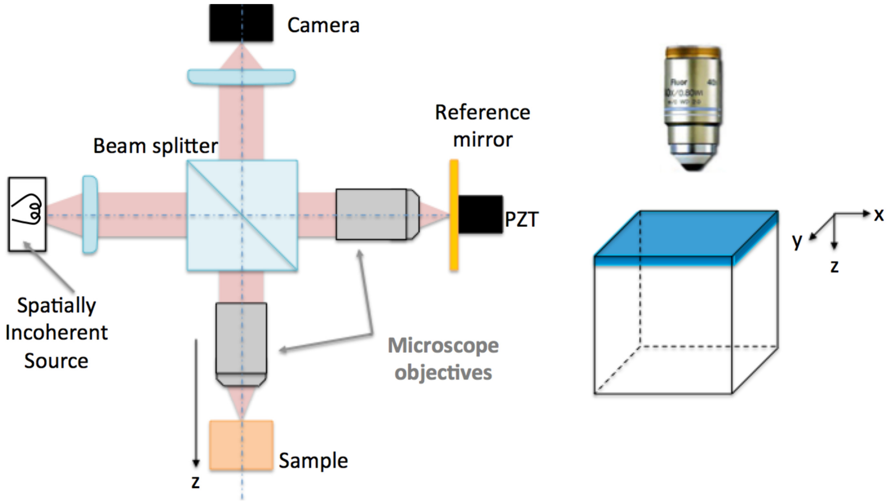

Fig. 3. FF-OCM principle using a Linnik interferometer [5]: A spatially incoherent source is focused on the sample. The microscope objective field of view is imaged on the camera. There is no need for an extended depth of field and high numerical aperture objectives can be used. *En face* flying spot scanning has also been used successfully with a single detector [25–27].

3. C-scan, full-field OCM or coherence holography?

When using optics of similar numerical aperture, we should be able to reach the same lateral resolution whatever the image acquisition system (i.e. flying spot C-scan or Full-Field OCM).

In terms of signal-to-noise ratio (SNR) the main difference between the various approaches is related to the energy available per voxel. We will suppose, and this is often the case in practice, that all the signals are *shot noise limited*. In order to provide a quantitative comparison between the different approaches we have to consider quantities such as source power, speed and complexity of the setup. Until recently 1 Mega-pixel cameras that have been used exhibit a typical full well capacity (FWC) of about 100 Ke-/pixel with speed around 100 frames/s meaning that they can only handle a low average power of about 0.1 mW for the field of view. A valuable improvement has been obtained recently with a specially designed camera made by Adimec within the framework of an EC project (CAReIOCA) led by LLTech [34]. This camera (500-700 frames/s, FWC of 2Me- and 2 Mega-pixel), can handle a power > 1mW. Because the reference signal can be damped without S/N losses, tens of mW could impinge on the sample.

This power is one to two orders of magnitude lower than SLDs or lasers used in scanning FF-OCM that have typical power of 10 to 100 mW. A gain of 10 to 20 dB is thus expected in terms of ultimate sensitivity.

In terms of speed, fast scanners can work at 10 to 100 KHz [35]. This corresponds to a time of 1/10 to 1/100 s for a 1 Mega-pixel B-mode image. If the acquisition times are now in the same range in terms of speed (voxel/s), as we mentioned the signal to noise ratio is expected to be higher with a flying spot system and a single detector that will not suffer from saturation as the camera pixels do.

Ultimately, the limit on power may be imposed by the sample itself: if skin can handle a few mW/mm^2 the most critical part of the body is the retina that cannot accept more than around one tenth of this value in the near infrared.

One has nevertheless to keep in mind that recording a full field with a camera is always much slower than recording a spectrum on a linear array (in Fourier or spectral domain OCT) and that in presence of sample motion, the signal could be lost as acquisition of multiple images is necessary to process the modulated signal. On the contrary each line of a B-scan can be correctly positioned in post-processing. This explains why only a limited number of in vivo studies have been done so far using FF-OCM on eye [36,37] or skin [38].

Another successful approach of *en face* imaging that has been coupled to broadband spatially coherent sources in order to perform sectioning is Holographic Coherence Imaging [39–41]. Instead of working in the image plane working in a Fourier plane offers a number of advantages, such as the possibility to record either on a fast photorefractive material or on a digital camera, to be shot noise limited even with noisy laser sources by spatial filtering, and finally to be able to capture single shot images avoiding the need for phase modulation [42,43].

4. Spatially coherent vs. incoherent sources: advantages and drawbacks

Going back to *en face* imaging, spatially coherent sources can be used to illuminate the field of view: they offer a number of advantages such as single shot imaging (i.e. without modulation [43] or easy dark field imaging [44] although dark field has recently been proven using incoherent sources [45]). Moreover, adaptive optics for aberration correction was coupled to OCT for better resolution of the retinal structure in B scans [46,47,49] and in C scans [48], and for correcting the wavefront in high-resolution 2 photon microscopy [50]. However Karamata et al. demonstrated experimentally and explained in depth in [51–53] that coherent illumination is a source of crosstalks that may quickly degrade the image quality. Crosstalk does not appear with incoherent illumination.

But as we mentioned in section 2 digital OCM using coherent sources for flying spot or full field is able to overcome not only the defocus problem but also to correct aberrations [19–24].

Here we will draw the attention of the reader to the role of spatial coherence: usually when scanning the field of view for a flying spot image, each acquisition (voxel or line) is an independent event and this is equivalent to an incoherent illumination. Surprisingly scanning and incoherent illumination are not equivalent in presence of aberrations: Indeed, in spatially incoherent full-field interferometer, the system PSF width is almost insensitive to aberrations and only the signal amplitude is reduced by the wavefront distortion (Fig. 4). This has been theoretically analyzed and compared with different coherent interferometers, and experimentally confirmed for defocus and random aberrations [54,55]. The unexpected unique merit of resolution conservation is only found in full-field spatially incoherent interferometer. If we consider the aberrated sample wavefront associated with a diffraction-limited spot in the sample arm in the presence of aberrations, the partial overlap with the corresponding diffraction spot reference wavefront damps the signal. Nevertheless the interferometric signal of the aberrated sample wavefront with a neighboring diffraction spot is damped to a greater extent. Indeed, the shift to the next spot is associated with a linear increase of $\pm 2\pi$ of the phase shift from one side of the pupil to the other. This supplementary phase shift increases the RMS value of the aberrated wavefront leading to a strong decrease of the signal for this neighboring point.

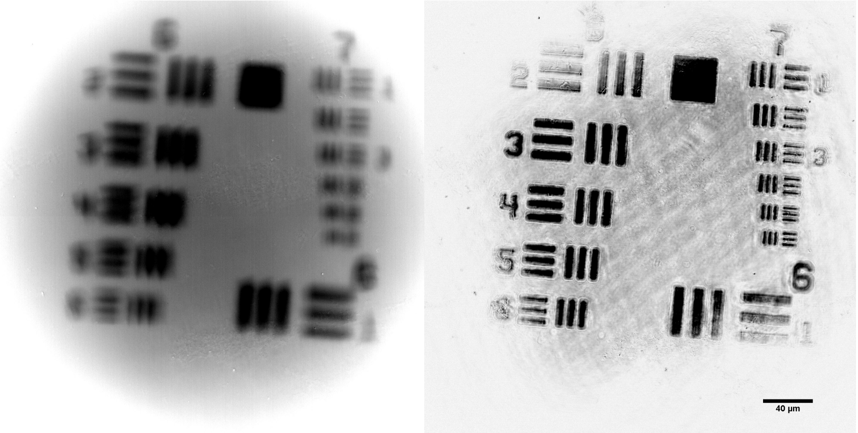

Fig. 4. The left image is the out of focus direct image of an USAF target. The right image is the same out of focus field obtained using FF-OCM: it clearly appears much less blurred (see text).

Finally, on considering the use of en face OCM compared to other techniques based on the use of optical contrasts, it appears that non-linear microscopy is most likely to compete with FF-OCM. Indeed the use of femtosecond lasers opens the way to both two photon endogenous fluorescence signals (from NADH in cell cytoplasm, that shows cell sizes and contours, and elastin fibers in connective tissue) and second harmonic generation that is mostly induced by the crystalline structure of various kinds of collagen. Collagen and connective tissue also contribute to the backscattered signals that are at the origin of the FFOCM signals; these rather strong signals often mask the low level of backscattered light from cells that only show up using dynamic FF-OCM (see section 5). As discussed in detail in reference [56], dynamic and static FF-OCM are complementary modalities that can be automatically superposed on the same field of view.

The table below intends to summarize the main features of typical OCT versus various typical OCM approaches.

	OCTs Spectral / Sw. source	OCM (Scanning)	OCM (Coh. illumination)	OCM (Incoh. illumination)
Axial: Transverse: Resolution	3 to 10 μm 10 μm	3 to 8 μm 0.5 to 2 μm	3 to 8 μm 0.5 to 2 μm	0.5 to 8 μm 0.5 to 2 μm
Speed (Pixels/s)	100 Gpixel/s	1-10 Gpixels/s >100 Gpixels/s with Spectral or Sw. source.	10-50 Gpixels/s 1 processed image	10-50 Gpixels/s 1 processed image
Sources	SLD/ Lasers (fs)	SLD/ Lasers (fs)	SLD/ Lasers (fs)	Thermal Sources LEDs
Typ. Power (sample) Sensitivity	10-100 mW 100/110 dB	10-100mW 100/110 dB	1 mW	0.5-2 mW 80-90 dB
Aberrations Corrections	With Adaptive Optics	With Adaptive Optics	With Adaptive Optics	No loss of resolution (only signal reduction)
Sensitivity to movements	Correction possible	Correction possible	Correction unlikely	Correction unlikely
Post-processing Depth of field and aberration correction	Synthetic aperture, Aberrations correction	Depth of field and aberration correction achieved	Numerically possible	Difficult
Main Drawbacks	Low resolution	Price of fs lasers	Crosstalks	Lower sensitivity: camera saturation. Sensitive to movements
Main Advantages	Broadly used Easy to implement	S/N. Coupling with non-linear microscopy	Possible wavefront shaping	Cheap, High resolution. Sub-cellular metabolism

5. Applications of *en face* tomo-microscopy: from diagnosis to art

As for the various OCT domains that have been studied over the past 25 years, *en face* OCM has mostly been devoted to medical diagnosis. Because *en face* imaging gives more flexibility in terms of lateral resolution, FF-OCM or C-scan OCM has targeted complementing histology for intra operative diagnosis [57–60]. With the new fast camera, 1cm^2 FF-OCM images with sub micrometer sampling (>100 Mega-pixel images) can be recorded within one minute with a suitable SNR [34]. A large number of images of different pathologies, mostly cancers [61,62], are available on the LLTech web site as well as a number of articles that demonstrate high levels of sensitivity and specificity, often over 90% [64].

We would like to provide here a few examples outside the well-covered field of medical diagnosis. *En face* OCT has been used for a number of biological applications competing with phase contrast microscopy [63]. For instance the kind of sectioning of the bed bug shown in Fig. 5 would have been impossible in transmission phase contrast microscopy.

OCT also proved very useful in material characterization and non-destructive testing [65,66], while FF-OCM with its high sensitivity and high sectioning ability was used to check local defects in optical interference coatings [67] and holography for analyzing various kinds of structures [39–41].

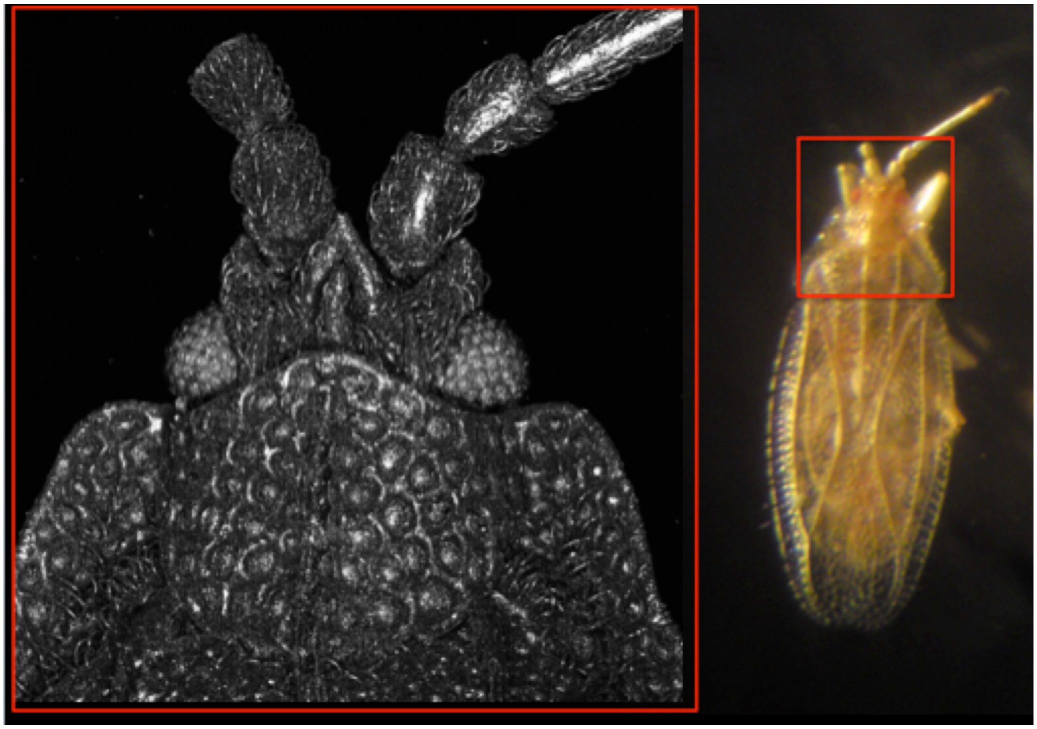

Fig. 5. FF-OCM of Bed bug *Tingis auriculata* left, and image of the whole bug on the right (field of view 1mm^2) fossilized in amber. Credit: Jean-Marie Chassot, Institut Langevin and Romain Garrouste, Muséum National d'Histoire Naturelle Paris.

At the limit between characterization and biometrics, OCT has been used to provide internal fingerprint images that cannot be counterfeited [68–71]. In the case of B-mode OCT an *en face* image must be deduced from a 3-D acquisition. On the contrary FF-OCM is able to directly capture the *en face* image of fingerprints [72] as can be seen in Fig. 6 where internal and external fingerprints are compared.

Fig. 6. In vivo FF-OCM of internal fingerprint (A) taken a few hundred micrometers below the skin surface and total reflection image of the same external fingerprint (inversed contrast). Credit: Egidijus Auktorius.

Even if biomedical applications of OCT dominate in terms of publications, the field of OCT for art is very active [73] and an up to date web site can be consulted [74]. As most art objects are designed for an *en face* view, FF-OCT seems a natural way to examine them.

Latour et al. used FF-OCM to analyze the structure of paint layers at high resolution [74] and various objects such as wood, lacquer (Fig. 7), amber etc. have been examined [75].

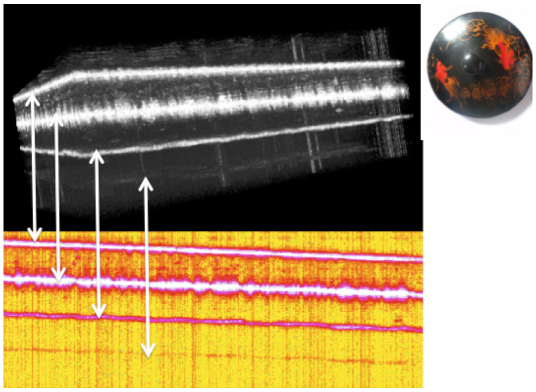

Fig. 7. 3-D Full Field OCT of the top of a lacquer pot. 4 layers can be observed here; more than 10 layers can be observed in antique lacquers.

6. Complementary endogenous and exogenous contrasts for *en face* microscopy

Despite worldwide success in the field of biomedical studies, OCT has often been associated with another modality in order to add information and to increase the sensitivity and specificity of the diagnosis.

En face fluorescence and coherence microscopy

As we have mentioned and we will see later many *en face* studies were inspired by similar preceding studies using OCT. On the other hand, to the best of our knowledge, the first multimodal imaging system that combined OCT and fluorescence was an *en face* one that mixed *en face* flying spot coherent microscopy with two photon fluorescence of calcium green dye [76] in rat brain. If OCT in general, and en-face OCT in particular, can provide a high-resolution, high sensitivity structural image of a tissue, it suffers from a lack of cellular and molecular specificity. Even performed with high numerical aperture objectives, *en face* OCT can only discriminate two cell populations based on their shapes, but not on their molecular content, or on their function. Fluorescence techniques can reveal or complement the OCT information that is obtained from a cell or a structure [77–80] using various approaches: single or 2 photon fluorescence, superficial observation or endoscopy [81–84]. Following similar developments in OCT [85–88], several multimodal setups associating full field microscopy and various fluorescence techniques have been developed [89–91]. While confocal or multi-photon microscopy can be naturally associated with point scanning OCT systems, it is less natural for full field coherence microscopy, where widefield fluorescence techniques are preferred. Therefore, most of the setups combining Full-Field OCM and fluorescence microscopy used Structured Illumination Microscopy (SIM) in the fluorescence channel to generate an optical section. This consists of conjugating a physical grid, often named a Ronchi ruling, with the focal plane of the objective. Fluorescent structures in focus are multiplied by the grid pattern intensity, whereas the grid is blurred outside of the focal plane. In this way, similarly to FF-OCM phase stepping, the out-of-focus fluorescence can be excluded by sequentially moving the grid in three, four, or multiple positions and computing the analog of the FF-OCM amplitude with similar algorithms. Ideally, two cameras are required for combining FF-OCM and SIM, as technological requirements of FF-OCM and fluorescence cameras are almost opposite. References [79] and [80] have proposed a similar configuration, in which a flip mirror enables acquisition of either an FF-OCT or a SIM image. Thanks to the sequential imaging of the two modalities, there are less spectral limitations for the two modalities combined. In practice, a white halogen lamp can illuminate the FF-OCM setup to provide an optical section as thin as 1 µm, while any kind of visible fluorophore can be used for fluorescence in parallel, because the two images are acquired one after the other. On the contrary [91], suggested a simultaneous configuration, in which a dichroic filter combines the fluorescence and the FF-OCM paths. Both modalities are therefore captured at the same time. This configuration can help to decrease the acquisition time, but the FF-OCM source and the fluorescence spectra should not overlap. We recently built a similar simultaneous configuration and demonstrated its interest for dynamic measurements including dynamic FF-OCM (see below) [92]. Moreover, using high NA objectives enabled us to rely on both the spatial optical sectioning, and the temporal optical sectioning [3]. Using this setup, structures invisible in FF-OCM were revealed [93,94]. With this multimodal setup, we have been able to add specific contrast to the structural FF-OCT image: Fig. 8 shows an example revealing nerves and nerve terminals at different depths in a mouse cornea using a fluorescent label that specifically labels nerves in a transgenic mouse line. In this example, FF-OCM can clearly identify the corresponding corneal layers and their associated structures that help to localize the nerves in 3D. We could show that most of the fine sub-basal nerves in the cornea were located at the surface of Bowman's layer, as expected from literature [95,96]. Interestingly, the thickest nerve fibers can be detected with FF-OCM at Bowman's layer, but it fails to detect thinner nerves, the nerve terminals, and most of the thick stromal nerves.

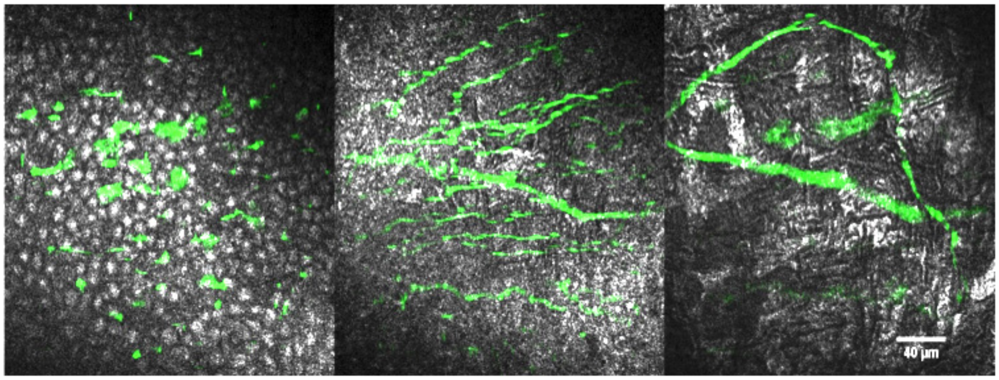

Fig. 8. Simultaneous FF-OCM and Fluorescence microscopy at different depths in a mouse cornea. The 3 panels show the overlay between the FF-OCM amplitude image and the fluorescence image collected from a nerve specific label in a transgenic mouse line. The 3 panels respectively represent typical images acquired respectively in the epithelium third layer (left), the Bowman's layer (middle), and at the top of the cornea stroma (right). FF-OCM can precisely identify the different layers of the cornea (basal epithelium left, Bowman's layer center, stroma right, with keratocytes visible as bright, star-shaped forms), but can reveal only a few nerves, whereas the fluorescence can reveal all the nerves and the nerve endings in the epithelium. The scale bar is 40 µm.

From blood flow to dynamic OCM

Motion is a key factor in living systems and one can use FF-OCM to assess the evolution of structures over time. Blood flow [97] can be seen and analyzed in this way and individual erythrocytes can be tracked if the frame rate of the camera is fast enough compared to the rate of flow of red blood cells [98]. Dynamic FF-OCM [99] aims to highlight another kind of motion, i.e. motion taking place inside cells and contributing to activity To extract dynamic FF-OCM signals, we record a short movie (about 1 second) of *en face* tomographic images and then process the time series obtained for each pixel. The fluctuations of the backscattered intensity are linked to the local metabolism inside the sample. Dynamic FF-OCM characterizes the local metabolism by the amplitude of the fluctuations and their characteristic time scale (Fig. 9).

We could also take advantage of this dynamic nature of the cells in fresh tissue to add new contrast in retinal imaging. Thanks to its high spatial resolution, FF-OCM can reveal valuable details in the retina [94]. Notably, in the ganglion cell layer, we are able to separate the contribution of the strongly scattering ganglion cell axons from that of the capillary walls, and from the weakest scattering structures, i.e. the cell somas.

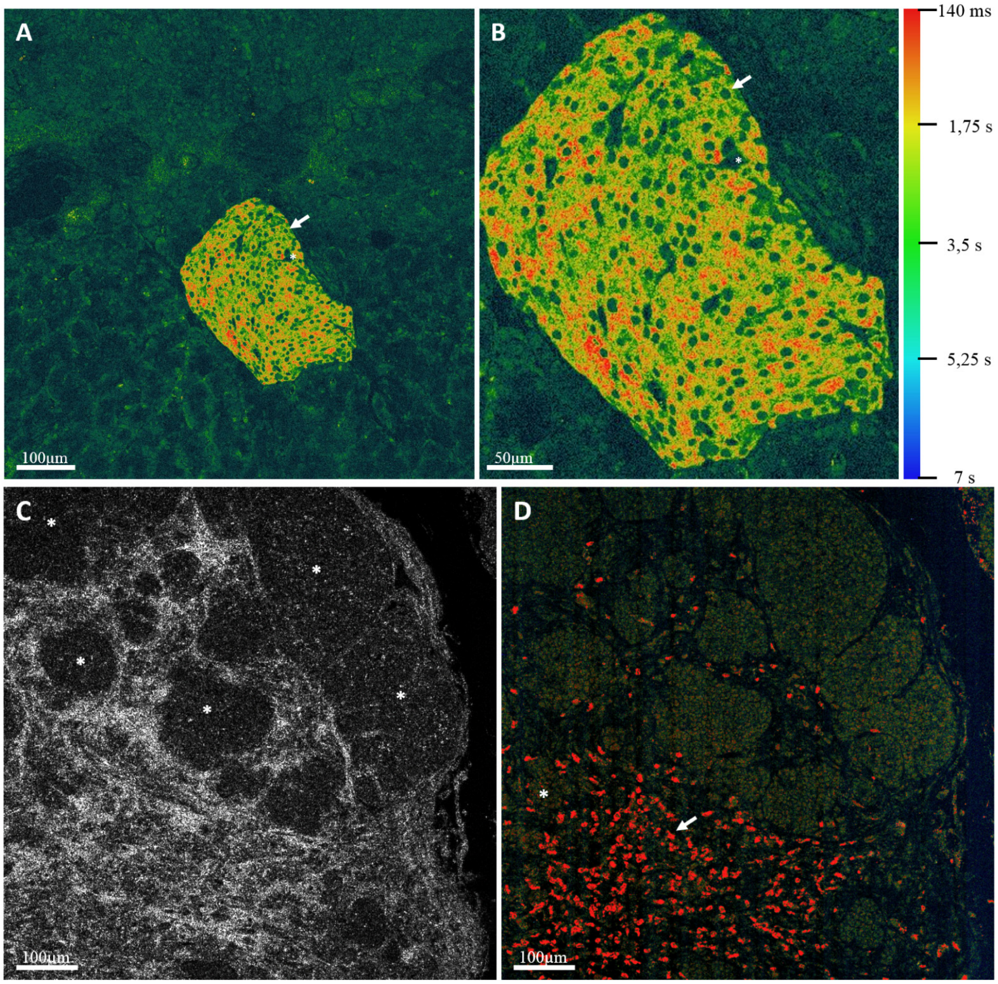

Fig. 9. (A) shows a Dynamic FF-OCM image of a Langerhans islet inside a fresh ex-vivo rat pancreas. One can notice the nuclei (arrow) with a circular shape and capillaries (*) irrigating the islet. (B) is a detailed view of the islet. (C) Shows the FF-OCM image a mouse intestinal tumor where the collagen matrix is highly visible compared to the cells inside the nests (*). (D) is a Dynamic FF-OCM image of the same field as (C), the collagen fibers are no longer visible because they are stationary, whereas the cancerous cells appear inside the nests and immune cells are revealed inside the collagen matrix (arrow). We also remove the ambiguity on zones like (*) and below where it was not clear if cancerous cells were present. The color bar is the same for the 3 images.

Figure 10 left presents a typical FF-OCM image of the retinal ganglion cell layer in mouse. First, as presented on the right in Fig. 10, simply looking at the amplitude of the temporal fluctuations, we can hide the signal from stationary axons and blood vessels and add an intracellular contrast, which allows the detection of some cell nuclei and enhances the signal from the red blood cells trapped inside the capillaries, thanks to their highly fluctuating membranes. One can then consider the relative frequencies of the temporal fluctuations. We can emphasize faster moving structures, or intracellular components. For example, in Fig. 10 center, we have created an RGB image from the slowly varying structures (< 0.5 Hz) displayed in red, the intermediate structures in green, and the fastest structures (>10 Hz) in blue. This display enables the identification of two cell populations: round cells with almost no intracellular inhomogeneity, and fewer cells with a faster cytoplasm, and a slower dark center, that could correspond to the nucleus. We postulate that these two cell populations could correspond to different cell types [96], which would offer a way to discriminate specific cells without labeling in live retinal explants.

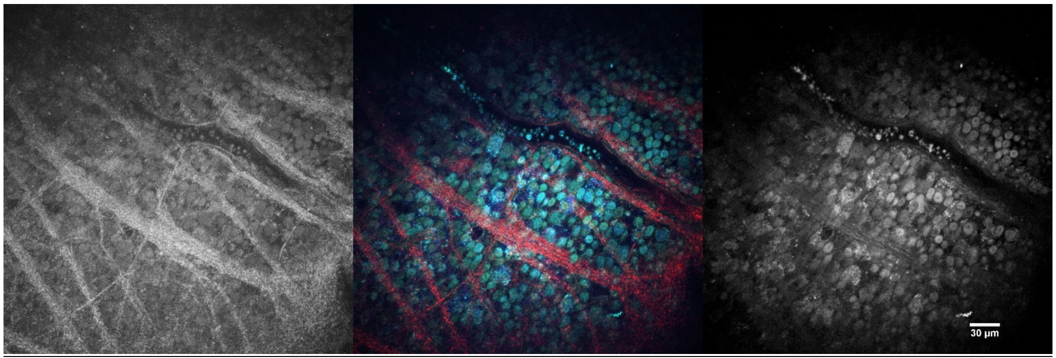

Fig. 10. Static and dynamic FF-OCM of the retinal ganglion cell layer in mouse. These panels display 3 different views of the same plane inside the ganglion cell layer of a mouse retinal explant, about 30 µm from the surface of the retina. 1000 images have been acquired without pizeo modulation at 100 frames per second, with a 40X, 0.8NA objective. The left hand panel presents the static contrast of this plane offered by FF-OCM. By taking advantage of the dynamics inside the living cells of this retina, we computed the Fourier transform of the temporal signal fluctuations. The center panel shows an RGB combination of different frequency bands: The red color represents the low temporal frequencies (<0.5 Hz), the green the intermediate frequencies (between 0.5 and 10 Hz), and the blue emphasizes the fastest pixels (>10Hz). The right hand panel is the same image as the blue component of the image in the center panel. The scale bar is 30 µm.

Whether using OCM [100] or Holography [101–103] we have to underline the importance of the dynamic approach and emphasize that similar dynamic approaches can track the evolution of cellular activity [104] or action of drugs [105,106] down to the nucleus scale [107].

Elastic properties

Knowing the elastic properties of tissues has proved to be valuable information to complement ultrasound imaging. Since the pioneering work of Schmitt [108] followed by the analysis of arterial stiffness of Bouma's group [109,110] an increasing number of studies combining OCT and elastography emerged [110]. For small strains, the variations in phase from usual B-scan images are sufficient to obtain the required information and *in vivo* experiments have been carried out successfully [111]. For a time dependent tissue deformation Doppler-like signal processing was used [111,112].

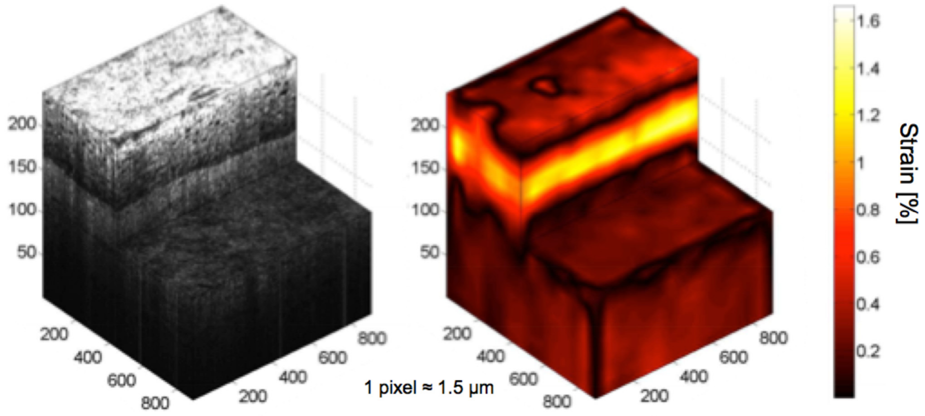

Fig. 11. OCM/elastography of artificial skin (Credit Amir Nahas).

However, in soft tissues, deformation occurs in 3D. 3D images are therefore recorded before and after deformation, and the strains are deduced from the 3D correlation of the two fields [113–115]. This was also the approach that we used using OCM at the micrometer scale, however, the effective resolution is unfortunately degraded by the correlation procedure [116].

A different way to measure stiffness is to induce strain waves that propagate through the tissue. This approach has been performed by a number of groups and often called dynamic OCT [117,118]. Surface waves [119,120] that could be generated without contact are often used for the cornea but also for tumor characterization [121]. We have used OCM coupled to an ultrafast camera to follow strain waves during their propagation [122].

All these dynamic studies are limited in terms of spatial resolution by the size and/or the frequency of the source that induces the waves.

We will end our examples of multimodal approaches; other examples can be found in reference 4 and include in particular photothermal effects that become important with the contrast induced by various kinds of nano particles [123,124].

7. Conclusion and perspectives.

We have tried in this article to review the main differences between *en face* and B-mode coherence imaging approaches; from the hardware point of view the most important point is the high lateral resolution, achieved by using high numerical aperture microscope objectives for *en face* imaging. We have then shown that full field coherence microscopy is able to capture millions of pixels images without scanning but carries drawbacks linked to the saturation level of cameras. Flying spot coherence microscopy is less limited in terms of usable power, flexibility to use Bessel beams etc.

Despite some notable technological progress, the frontline of the field, in our opinion, lies rather in the mathematical/digital methods that improve SNR and available depth, along with the possibility of adding complementary contrasts to the OCT/OCM morphological information.

Concerning the complementary contrasts we have pointed out a number of fields of application where *en face* images are more likely to be used and shown that, as in B scan approaches, multimodal imaging using a combination of contrasts is highly valuable to complement the structural information that we usually obtain.

Nevertheless, a major limitation of FF-OCM compared to B-scan OCT remains its penetration depth. Along with peers involved in coherent imaging, we think that this limitation on accessible imaging depth is due to multiple scattering that happens in highly scattering media [125,126]. Confocal filtering in flying spot OCT acts as a filter for the multiscattered light but an equivalent filtering happens in (33) in full field detection. The fact that *en face* OCM is more sensitive to multiple scattering is linked to the geometrical aberrations that are more likely to show up at large aperture. Indeed it is demonstrated [130, supplementary] that, at a given depth, the ratio of Single-Scattering/Multiple-Scattering scales as the Strehl ratio (diffraction limited PSF area/aberrated PSF area). If we consider low order aberrations such as defocus or spherical aberration, the wavefront distortion scales as the square or the forth power of the numerical aperture. Because of the associated damping of the ballistic photons it is then more likely that multiple scattering affects large numerical aperture experiments.

Inspired by experiments in ultrasonic acoustics [116–118], based on the acquisition of a time dependent reflection matrix and theory based on singular value decomposition of this matrix, an en face microscopy matrix approach to optical imaging has recently been proposed. The aim of such an approach that is able to more efficiently filter the multiple scattered light is to push back the imaging depth limit [119]. By combining matrix discrimination of ballistic waves and iterative time reversal, it was demonstrated both theoretically and experimentally that an extension of the imaging-depth limit by a factor larger than two was possible, rendering greater depth than OCT attainable while keeping the transverse resolution of OCM.

Funding

This work was supported by grants from the European Research Council SYNERGY Grant scheme (HELMHOLTZ, ERC Grant Agreement# 610110; European Research Council, Europe) and LABEX WIFI (Laboratory of Excellence ANR-10-LABEX-24) as part of the French Program ‘Investments for the Future’ under reference ANR-10-IDEX-0001-02 PSL.

Acknowledgments

We warmly thank Egidijus Auksorius for the fingerprint images, Jean-Marie Chassot and Romain Garrouste for the bug OCM images, Nacim Bouheraoua and Djida Ghoubay for the corneal and retinal tissues.